arXiv:astro-ph/9805218v1 15 May 1998

The Galaxy Luminosity Function at $z \leq 0.05$: Dependence on Morphology

Ronald O. Marzke[1]
Carnegie Observatories, 813 Santa Barbara St., Pasadena, CA 91101
and
Dominion Astrophysical Observatory, Herzberg Institute of Astrophysics, National Research Council of Canada, 5071 W. Saanich Rd., Victoria, BC, Canada V8X 4M6

L. Nicolaci da Costa[2]
European Southern Observatory, Karl-Schwarzchild-Strasse 2, 85748 Garching bei Munchen

Paulo S. Pellegrini and Christopher N.A. Willmer
Departamento de Astronomia CNPq/Observatorio Nacional, Rua General Jose Cristino, 77, Rio de Janeiro, Brazil 20.921

Margaret J. Geller
Harvard-Smithsonian Center for Astrophysics, 60 Garden St., Cambridge, MA 02138

ABSTRACT

We investigate the dependence of the local galaxy luminosity function on morphology using 5,404 galaxies from the recently enlarged Second Southern Sky Redshift Survey (SSRS2). Over the range $-22 \leq M_B \leq -14$ ($H_0 = 100$ km s^{-1} Mpc^{-1}), the luminosity function of early-type galaxies is well fitted by a Schechter function with parameters $M_* = -19.37^{+0.10}_{-0.11}$, $\alpha = -1.00^{+0.09}_{-0.09}$ and $\phi_* = 4.4 \pm 0.8 \times 10^{-3}$ Mpc^{-3}. The spiral luminosity function is very similar and is well fitted by the parameters $M_* = -19.43^{+0.08}_{-0.08}$, $\alpha = -1.11^{+0.07}_{-0.06}$ and $\phi_* = 8.0 \pm 1.4 \times 10^{-3}$ Mpc^{-3} over the same range in absolute magnitude.

The flat faint end of the early-type luminosity function is consistent with earlier measurements from the CfA Redshift Survey (Marzke *et al.* 1994a) but is significantly steeper than the slope measured in the Stromlo-APM survey (Loveday *et al.* 1992). Combined with the increased normalization of the overall LF measured from intermediate redshift surveys, the flat faint-end slope of the E/S0 LF produces no-evolution models which reproduce the deep HST counts of early-type galaxies remarkably well. However, the observed normalization of the SSRS2 LF is consistent with the low value measured in other local redshift surveys. The cause of this low-redshift anomaly remains unknown.

---

[1]Hubble Fellow

[2]Also Departamento de Astronomia CNPq/Observatorio Nacional, Brazil

The luminosity function of irregular and peculiar galaxies in the SSRS2 is very steep: $M_* = -19.78^{+0.40}_{-0.50}$, $\alpha = -1.81^{+0.24}_{-0.24}$ and $\phi_* = 0.2 \pm 0.08 \times 10^{-3}\,\mathrm{Mpc}^{-3}$. The steep slope at the faint end is consistent with the LFs measured for Sm-Im galaxies in the CfA survey, UV-selected galaxies (Treyer *et al.* 1997), star-forming field galaxies (Bromley *et al.* 1997) and the bluest galaxies in the SSRS2 (Marzke & da Costa 1997). As shown by Driver, Windhorst & Griffiths (1995*b*), the steep LF reduces the observed excess of faint irregulars over no-evolution predictions but cannot explain it entirely.

Subject headings:

1. Introduction

The luminosity function (LF) of low-redshift galaxies is a primary benchmark for models of galaxy formation. The detailed shape of the LF reflects a host of physical processes ranging from the collapse of dark-matter halos to the complex cycle of gas cooling, star formation, and feedback into the interstellar medium. The dependence of the LF on other observables such as morphology, color and emission-line strength provide further constraints on the input physics. Along with dynamical measures of galaxy masses, the LF for various types along the Hubble sequence anchors the theory of galaxy formation at low redshift.

Deep counts and redshift surveys of faint galaxies provide a wealth of constraints on galaxy evolution. Although recent surveys have been designed to cover a wide range in redshift and apparent magnitude (*e.g.*, Lilly *et al.* 1995 and Ellis *et al.* 1996), limits on available telescope time force a compromise between the redshift baseline and the sampling at each redshift. Surveys targeting intermediate-redshift galaxies are inevitably quite sparse at redshifts less than $z \approx 0.1$. The Autofib survey (Ellis *et al.* 1996) is perhaps the best compromise; the solid angle of that survey decreases with limiting magnitude in order to produce a catalog with similar numbers of galaxies in each broad redshift bin. However, in the regime $z \leq 0.1$, wide-angle surveys at relatively bright apparent magnitudes remain the best approach for measuring the local LF and its variations from one part of the local universe to another.

Very local samples ($z \leq 0.05$) allow the most detailed investigations of individual galaxy properties at the present-epoch; nearby galaxies are conveniently large and bright. The cost of this acuity is the unavoidable fact that smaller volumes are less likely to be fair samplings of the universe. Because fluctuations in the density field decrease with scale, samples covering larger volumes yield better estimates of the galaxy density. Furthermore, the properties of individual galaxies correlate with local density on relatively small scales (Dressler 1980, Postman & Geller 1984, Maia & da Costa 1990, Hashimoto *et al.* 1997). Correlations between galaxy properties and density on large scales are only vaguely understood (Park *et al.* 1994, Willmer, da Costa & Pellegrini 1997), but it seems clear that fair estimates of the local LF and its dependence on

galaxy properties requires averaging over a large number of large-scale structures. Limits to our knowledge of the present-epoch universe are fundamental: in order to resolve the evolutionary history of the galaxy population from $\sim 1\,\mathrm{Gyr}$ ago up to the present day, we are consigned by light-travel time alone to a region $\sim 600h^{-1}\,\mathrm{Mpc}$ across.

Recent HST surveys of faint field galaxies have opened new windows on galaxy morphology at high redshift (Driver *et al.* 1995*a*, *b*, Glazebrook *et al.* 1995, Abraham *et al.* 1996). Because different types of galaxies have quite different spectral energy distributions, apparent magnitude-limits impose redshift-dependent filters upon the observed distribution of galaxy types. Predictions of the morphological composition of intermediate and high-redshift samples require (at the very least) a detailed understanding of the distribution of morphologies nearby.

In this paper, we measure the luminosity function and its dependence on galaxy morphology using the 5404 galaxies in the combined SSRS2 samples in the northern and southern Galactic caps. We summarize the data in §2 and review our computational techniques in §3. Section §4 summarizes the results, and in §5 we discuss the implications for deep HST counts. We conclude in §6.

2. Data

The details of the SSRS2 southern sample have appeared in other papers (Alonso *et al.* 1993a,b, da Costa *et al.* 1994, Marzke & da Costa 1997). The sample has since been enlarged to include 1,937 galaxies from the northern Galactic hemisphere. A comprehensive description of the full sample may be found along with the entire SSRS2 catalog in da Costa *et al.* (1998). The photometric sample is generated from the non-stellar sources of the STScI Guide Star Catalog (GSC hereafter, Lasker *et al.* 1990). Galaxies were distinguished from stars, HII regions and other contaminants first by matching with existing galaxy catalogs and then by careful examination of each unmatched source by eye. The algorithm for determining local sky background in the GSC imposed a maximum size for galaxy detection. This size was appoximately $10'$. Galaxies larger than this make up a very small fraction of the magnitude-limited sample, but for completeness, they were inserted into the catalog by hand using the Morphological Catalog of Galaxies (Vorontsov-Velyminov & Karanchentsev 1963-1969) and the ESO Surface Photometry Catalog (Lauberts & Valentijn 1989). It should be noted that the exclusion of very large galaxies is endemic to large plate surveys such as the APM (Maddox *et al.* 1990) and COSMOS (Heydon-Dumbleton *et al.* 1989). The magnitude system is calibrated with CCD photometry in Alonso *et al.* 1993a,b, where the magnitudes b_{SSRS2} are defined to match the B(0) system used in the CfA Survey as closely as possible. In practice, b_{SSRS2} turns out to be very close to the flux within the 26 mag arcsec^{-2} isophote, or B_{26} on the ESO-LV system. The full sample now includes redshifts for all 5,426 galaxies brighter than $m_{SSRS2} = 15.5$ over 1.69 steradians of the southern sky. The boundaries of the survey are defined as follows: $-40^\circ \le \delta \le -2.5^\circ$ and $b_{II} \le -40^\circ$ for SSRS2 South, $\delta \le 0^\circ$ and $b_{II} \ge 35^\circ$ for SSRS2 North. Because the sampling beyond $z = 0.05$ becomes

somewhat sparse, we restrict our computations of the luminosity function to $z \leq 0.05$.

Morphological classifications in the SSRS2 come from several sources. The accuracy of the types varies from the detailed morphologies of Corwin *et al.* (1985) to rough designations assigned by one of the authors (PSP) using film copies of the ESO B plates (and in some cases with further examination of SERC J copies). The various sources and the modifications required to establish a homogeneous system are described in detail in da Costa *et al.* (1997). The Corwin morphologies are accurate to approximately one de Vaucouleurs T type, while the roughest classifications distinguish only the principal types: E, S0, spiral, and irregular. For the purposes of this paper, we smooth all the classifications into three broad categories in order to assure a consistent morphological scale: E/S0, spiral, and irregular/peculiar/interacting. Only 22 of the 5426 SSRS2 galaxies could not be classified on this scale. In order to give some idea of the accuracy of our morphologies, we show a representative range of galaxies at each morphology in Figure 1. The three columns contain (from left to right) the best, typical, and worst examples of each type of galaxy in the SSRS2. The "best" and "worst" candidates were chosen to represent roughly the best and worst 10% of the sample. It is clear that in the "difficult" bin, the finer classifications blur; for example, faint irregulars may be labeled peculiar and *vice versa*. However, even for these very faint galaxies, the distinction between E/S0, spiral and irregular/peculiar/merger is still relatively straightforward. We discuss the possible effects of classification errors in §5.

3. Technique

We compute the luminosity function for different morphological types using the maximum likelihood techniques of Sandage, Tammann & Yahil (1979, hereafter STY) and Efstathiou, Ellis & Peterson (1988, hereafter EEP). In the STY approach, we fit a Schechter function to each luminosity function

$$\phi(M) = 0.4 \ln 10 \, \phi_* [10^{0.4(M_*-M)}]^{1+\alpha} \exp[10^{0.4(M_*-M)}]$$

by maximizing the likelihood $\mathcal{L}$ that all sample galaxies appear in a magnitude-limited redshift survey,

$$\mathcal{L} = \prod_{i=1}^{N} \frac{\phi(M_i)}{\int_{-\infty}^{M_{min}(z_i)} \phi(M) \, dM}$$

Here, each M_i is a measured absolute magnitude (corrected for Galactic extinction and the K-correction at z_i), and $M_{min}(z_i)$ is the faintest observable absolute magnitude given the redshift of galaxy i, the K-correction at that redshift, the Galactic extinction and the apparent magnitude limit of the sample. The type-dependent K-corrections come from the model spectral energy distributions of Rocca-Volmerange & Guiderdoni (1988), and extinction corrections are $4.0E(B-V)$ using the reddening measurements of Burstein & Heiles (1982). We compute all distances using $H_0 = 100$ km s^{-1} Mpc^{-1} and $q_0 = 0.2$. At these low redshifts, q_0 has little effect on the computed absolute magnitudes; our choice is meant to reflect recent observational constraints

on the value of the mean mass density and does not include any contribution from a cosmological constant. Because of possible distance errors, we ignore all galaxies with Hubble velocities less than 500 km s^{-1} after correction to the local group barycenter. We investigate residual effects of local peculiar velocities in §3.

Because the normalization of the LF drops out of the likelihood function, the STY technique yields unbiased estimates of the shape parameters M_* and α even in the presence of large density inhomogeneities (as long as the Schechter function is a reasonable match to the shape of the LF and the correlations between the LF and the density field are weak). We compute confidence intervals on the shape parameters by computing the locus of points in the M_*-α plane where $\ln \mathcal{L}_\beta = \ln \mathcal{L}_{max} - \chi_\beta$, where χ_β is the beta point of the χ^2 distribution (EEP). Finally, we compute the normalization ϕ_* using the minimum-variance estimate of the mean density in redshift shells (Davis & Huchra 1982). Because there are large density fluctuations on the scale of the SSRS2, we simply compute the mean value of ϕ_* between 3,000 and 12,000 km s^{-1} in bins of 500 km s^{-1}. We compute the uncertainty in the mean by combining the standard deviation of density estimates in the redshift histogram with the uncertainty in the selection function.

The stepwise maximum-likelihood method of EEP approximates the LF as a set of step functions. The values of the steps at each absolute magnitude form the set of fitted parameters (EEP, Loveday *et al.* 1992, Marzke *et al.* 1994*a*,Marzke, Huchra & Geller 1994*b*, Lin *et al.* 1996, Heyl *et al.* 1997). Once again, the shape of the LF is determined independently of the density field. In this approach, error bars on each step come from the diagonal elements of the inverted information matrix, which consists of second derivatives of the likelihood function.

4. The Luminosity Functions

Figure 2 shows LFs for the three broad galaxy classes discussed in §2: E/S0, Spiral and Irregular/Peculiar. The dashed line also gives the LF of the combined sample. Confidence intervals for the Schechter shape parameters appear in Figure 3, and the first four rows of Table 1 list the fitted parameters along with 1σ errors. The fitted SWML parameters are listed in Table 2 along with the number of galaxies in each bin. Note that the redshift and absolute magnitude limits reduce the total number of galaxies used in the LF computation to 5,036. Two conclusions are immediately evident from Figures 2 and 3. First, the faint end of the E/S0 LF is flat ($\alpha = -1.00 \pm 0.09$) to the absolute magnitude limit of our survey, $M_B = -14$. Second, the irregular/peculiar LF is steep: $\alpha = -1.81 \pm 0.24$. As we will discuss in the next section, both of these conclusions are relevant to the interpretation of deep galaxy counts. Before we proceed, however, it is worth looking more carefully at some of the systematic uncertainties affecting these luminosity functions.

The faint end of the luminosity function of any type of galaxy is notoriously difficult to measure. In a magnitude-limited redshift survey, intrinsically faint galaxies represent a tiny

fraction of the final sample. The faintest galaxies can only be detected in a relatively small, nearby volume which is subject to large density fluctuations. A further complication in the analysis of very nearby galaxies is the distance uncertainty introduced by peculiar velocities. Although uncertainty in the Hubble constant alone does not affect the *shape* of the luminosity function, systematic deviations from the Hubble flow certainly can.

The redshift maps in Figure 4 demonstrate some of these difficulties. In this figure, right ascension is the angular coordinate, and the radial coordinate represents redshift. The left column shows the entire redshift range; the center of the circle is $cz = 0$ and the outer boundary is $cz = 20,000$ km s^{-1}. Figure 4*a* shows the declination range $-40° \leq \delta \leq -20°$ while Figure 4*c* shows the range $-20° \leq \delta \leq 0°$. We include these plots to give an idea of both the characteristic structures and the boundaries of the survey (because of the broad slices in declination, the Galactic latitude cut is difficult to show directly). The right-hand column is an expanded view of the region $cz \leq 3,000$ km s^{-1}, which is roughly the depth to which a galaxy with $M_B = -17$ can be seen given the magnitude limit of the survey. As expected, the density field is highly non-uniform on this scale. Two features of the galaxy distribution are particularly relevant to our measurement of the faint end of the LF. First, the dominant feature at very low redshift is the void in SSRS2 South (22^h-3^h, $cz \leq 1,500$ km s^{-1} in Figures 4*b* and *d*). Because of this underdensity, the number of galaxies with $M_B \geq -15.5$ is quite small (48 galaxies with $cz \geq 500$ km s^{-1}). The second feature is the obvious overdensity between 3^h and 4^h in Figure 4*b*. panel ($cz \approx 1,100$ km s^{-1}). This region includes the Fornax and Eridanus clusters, where virial motions are large and therefore individual galaxy distances are uncertain. If a significant fraction of the intrinsically faint galaxies are bound to these clusters, then we may expect some systematic error in the faint end of the LF both from the incoherent velocity fields within the clusters (i.e. the redshift fingers) and from the coherent streaming motions induced by the large-scale density fluctuations.

In order to evaluate the effects peculiar motions, we explore two cases. First, we compute the LF using a simple model for the local flowfield: we assume spherical infall to the Virgo cluster with $v_{inf} = 250$ km s^{-1} (case 1). Although this case clearly ignores very local flows such as infall to Fornax, it serves as a good starting point. In the second case, we again assume spherical infall to Virgo but add the somewhat extreme assumption that all galaxies lying within 1.5 h^{-1} Mpc (projected) and $2,500$ km s^{-1} of the centers of known clusters actually lie at the central redshift of the clusters. Although these cases are not exhaustive, they should give us some idea of the degree to which peculiar velocities affect our conclusions.

Figure 5 shows the LFs computed in cases (1) and (2) along with the original LFs shown in Figure 2. For reference, the fitted Schechter functions are recorded in the last eight rows of Table 1. Although the general result of the Virgocentric flow correction is to make galaxies brighter, the effects on the shape of the overall luminosity function are quite small (panel *a*). This result is not surprising: since the mass concentration driving the flow sits in the northern hemisphere, the flow in the SSRS2 region is essentially a bulk motion where all galaxies move in roughly the same direction. A small inflection appears at $M_B = -15.5$ after the correction, and the number in the

very faintest bin decreases by approximately a factor of two (roughly the size of the original 1σ error bar). Because the spirals are well dispersed through the volume, it is also not surprising that the effects on the spiral LF are small (panel *c*). A similar inflection appears at $M_B = -15.5$, but again the new LFs are consistent with the original estimates to within the 1σ errors. Because of the presence of the clusters, one might expect the case (2) corrections to have the greatest impact on the E/S0 LF. However, panel (*b*) shows that even the extreme assumption that all galaxies near Fornax and Eridanus are in the cluster cores does not change the LF significantly. Finally, because most irregular/peculiar galaxies are faint, one also expects their LF to be particularly sensitive to local flows. Once again, the changes in the LF are small. The case of pure Virgocentric flow reduces the number of irregular/peculiar galaxies brighter than L_* somewhat, but overall, the luminosity functions are all consistent. The steep Schechter function is a reasonable approximation to the irregular/peculiar LF no matter what we assume for the local flow field: the shallowest LF (case 1) has a faint-end slope $\alpha = -1.74 \pm 0.25$. The slope appears to be somewhat flatter if we consider only galaxies fainter than $M_B = -18$, but even in this magnitude range, the slope is still $\alpha \approx -1.5$. We show a Schechter function with this shallower slope as the dashed line in Figure 5. Although this function is a very poor fit to the rest of the luminosity function, it serves as a representative lower limit to the slope at the very faint end. We conclude that our luminosity functions depend only weakly on the details of the local flow field.

The SSRS2 LFs closely resemble the LFs derived for similar morphological classes in the CfA Survey (Marzke *et al.* 1994a) but disagree in some cases with those derived from the Stromlo-APM (Loveday *et al.* 1992). In the SSRS2, the faint end of the Irr/Pec LF is much steeper than in any other class of galaxies. Our best estimate of the slope is $\alpha = -1.81 \pm 0.24$, quite similar to earlier measurements from the CfA: $\alpha = -1.88 \pm 0.2$. As with the other morphological classes, however, the Irr/Pec M_* is considerably brighter in the SSRS2 than in the CfA Survey, and ϕ_* is consequently lower. In Figure 6, a direct comparison of the luminosity functions shows that the faint ends of the Irr/Pec LFs match remarkably well; the difference between the two stems from a decrement of bright galaxies in the CfA survey (or possibly an excess in the SSRS2). Unfortunately, irregular and peculiar galaxies were combined with spirals in Loveday *et al.* (1992), and we cannot compare our results to the Stromlo-APM directly.

The LF of early-type galaxies in the SSRS2 is essentially flat between M_* and $M_B = -14$: $\alpha = -1.00 \pm 0.09$. At faint absolute magnitudes, the E/S0 LF significantly exceeds the Stromlo-APM LF (Loveday *et al.* 1992) but is similar to the CfA LF (see Figure 6). Again, however, the CfA LF shows a deficit of bright E/S0's compared to the SSRS2. The overall normalization of the CfA E/S0 LF is also somewhat higher than the SSRS2 even at the faint end. This excess of CFA E/S0s is consistent with the enhanced abundance of clusters in the CfA sample, most of which are concentrated in the northern Galactic cap (Ramella *et al.* 1997, Marzke *et al.* 1995).

The deficit of bright galaxies in the CfA LFs appears consistently in each morphological bin and probably signals a systematic error in the Zwicky system. The source of the discrepancy at the bright end between the CfA survey and nearly every other survey is unclear; systematic errors

in the Zwicky magnitude scale remain poorly constrained. One might suppose that saturation in the Schraffierkassette films used in the Zwicky Catalog (on which the CfA Survey is based) could lead to underestimation of the flux in bright galaxies. However, intrinsically bright galaxies appear over a wide range of *apparent* magnitudes in the CfA sample, and it is not immediately clear that saturation could cause the observed depression at the bright end of the LF. The CfA LF could also be forced to agree with the SSRS2 by convolving an extra Gaussian error distribution with $\sigma \approx 0.5$mag (in addition to the 0.35 magnitude error computed by Huchra (1976) and already deconvolved during the computation of the LF). In this case, however, it is not clear where such a large dispersion would arise; random errors in the SSRS2 and CfA magnitudes are quite similar. A definitive resolution of this problem awaits the completion of wide-angle CCD surveys (e.g. Gunn 1995), which will provide more accurate magnitudes for CfA (and maybe later SSRS2) galaxies and will provide a more detailed understanding of the completeness of local redshift catalogs.

5. Reconciling Galaxy Counts with the $z = 0$ LF

Three aspects of the local luminosity function are particularly relevant to the interpretation of intermediate-redshift morphology. First, the overall normalization of the present-epoch LF affects the predicted galaxy counts for all morphological types and is an important factor in the debate over very recent galaxy evolution. Second, the faint-end slope of the E/S0 LF plays a critical role in the debate over the age and formation history of early-type galaxies. Because the deep number counts of early-type galaxies differ least from no-evolution predictions, the shape of the local LF has the largest effect on the inferred evolution. Finally, the abundance of local irregulars and the shape of the irregular-galaxy LF are important to our understanding of the remarkable irregularity observed in the faint blue galaxy population. In the following sections, we focus on each of these aspects individually.

5.1. Normalization

Maddox *et al.* (1990) were the first to draw attention to the remarkably bright apparent magnitude at which the observed galaxy counts diverge from no-evolution predictions. They interpreted their results as evidence of very recent evolution in the galaxy population. Since then, the steep galaxy counts at $B \leq 20$ have been ascribed to a number of alternative sources including large-scale density fluctuations, scale errors in the APM magnitudes and systematic errors in the APM galaxy detection. Given the uncertainty in the plate surveys, is it reasonable to predict faint galaxy counts using luminosity functions derived from bright galaxy redshift surveys? In this section, we attempt to address this question quantitatively.

Although we can measure the *shape* of the luminosity function accurately even in the presence of large density fluctuations, our *normalization* is fixed by the galaxy counts to our limiting

magnitude and is therefore sensitive to local density anomalies. Large-scale structure affects the counts when galaxies cannot be seen to distances much larger than the size of the structure. At $B = 15.5$, the observable redshift range is only a few times the typical void size. At even brighter magnitudes, we expect the observed counts to exceed the predictions of a homogeneous model simply because our viewpoint is not a random one: other galaxies are correlated with our own.

Figure 7 shows the SSRS2 galaxy counts (solid triangles) along with the predictions based on the overall luminosity function from Table 1, k-corrections for an Sb galaxy (an appropriate mean for a B-selected sample at this depth), our chosen cosmological parameters: $H_0 = 100, q_0 = 0.2$, and an assumed dispersion in the photometry of 0.3 magnitudes (solid line). Because the normalization of the LF is largely determined by galaxies fainter than $B = 14.5$, it is not surprising that the predicted counts agree well with the observations at these magnitudes. Even so, fluctuations caused by large-scale structure are apparent even at $B = 15.0$; in this case, the excess in the counts is caused by the overdensity of galaxies at approximately 6,000 km s^{-1} previously labeled the Southern Wall (da Costa *et al.* 1998; also see Figure 4). As expected, local clustering also flattens the slope of the observed counts at brighter magnitudes. At the magnitude limit of the survey, the agreement between the observed and predicted counts is excellent.

The open circles in Figure 7 represent the APM counts from Maddox *et al.* (1990). As they pointed out, the counts depart from the no-evolution predictions at approximately $B = 17$. It is worth pointing out that in the small region of overlap ($B \approx 15.5$), the SSRS2 counts reproduce the APM counts very well. The construction of the SSRS2 photometric catalog does not force this agreement; initial candidates for the SSRS2 included all sources flagged as non-stellar in the STScI scans of the SERC J plates. Although both surveys share the same original plate material, the STScI survey is based on PDS scans with a higher dynamic range, and algorithms for detection and photometry were constructed independently.

Given the recent reports of possible scale errors in the APM (Metcalfe *et al.* 1995, Bertin & Dennefeld 1997*a*), the agreement between the APM and the SSRS2 (which is independently calibrated using extensive CCD photometry) may seem surprising. However, the reported problems in the APM appear primarily at fainter magnitudes than are probed by the SSRS2: $16 \leq B_J \leq 18$. Metcalfe *et al.* (1995) claim that the low APM counts at magnitudes brighter than this (and therefore in the range of the SSRS2) cannot be explained by the same errors. On the other hand, Bertin & Dennefeld (1997*a*) attribute their lower counts at $B_J \leq 16$ to incompleteness in their photographic catalog, and they caution that similar incompleteness affects other photographic surveys as well. They identified star/galaxy separation as the primary culprit behind their incompleteness at the bright end. It is important to point out, however, that the SSRS2 grew out of the nonstellar sources of the STScI Guide Star Catalog, where the definition of "nonstellar" is necessarily conservative. Because the astrometric requirements of the HST were the primary consideration in the construction of the GSC, Lasker *et al.* (1990) tuned the stellar classifier to assure a clean *stellar* catalog. Even so, roughly 2% of the SSRS2 galaxies were originally classified as stars in the GSC but were labeled galaxies in the APM, ESOLV or MCG (da Costa *et al.*

1998). This fraction is consistent with the success rate established by Lasker *et al.* (1990) using visual checks and multiply observed sources. Because stars at this apparent magnitude are very numerous compared to galaxies, it is of course possible that some galaxies were left for stars in all four catalogs and therefore did not make it into the final version of the SSRS2.

The number of very compact galaxies missed in the bright galaxy counts can only be resolved by blind redshift surveys of all detected sources in a field. At these magnitudes, the large ratio of stars to galaxies is a major obstacle. Although we lack strong observational constraints, we can roughly gauge the magnitude of the problem using theoretical predictions of the distribution of galaxy sizes. Such predictions relate the surface brightness profiles and rotation curves of galaxy disks to the distributions of mass and angular momentum in the parent dark-matter halos (Dalcanton, Spergel & Summers 1997, Mo, Mao & White 1997). Because these models are reasonably successful at matching the properties of galaxies we see, they may provide some useful clues about those we don't. Here, we are particularly interested in the distribution of scale lenghts at a fixed halo mass (in this case the mass corresponding to an L_* galaxy, $\sim 10^{12} M_\odot$), which depends only on the distribution of angular momenta. Using reasonable parameters for the distribution of halo angular momenta and the baryon fraction as outlined in Dalcanton *et al.* (1997), we find that the the fraction of L_* galaxies with scale lengths less than a kiloparsec (which corresponds roughly to the size of the point-spread function at the maximum depth of the SSRS2) is smaller than 10% if $\Omega_0 = 1$. At lower Ω_0, the fraction is even smaller. Of course, these models are only a first step and require further testing, but to first order, we expect a very small error in the density of L_* galaxies from misclassification of compact galaxies.

At the other end of the surface-brightness spectrum, we also expect some bias against very diffuse galaxies in the SSRS2. As originally suggested by Disney (1976), local surveys of low-surface-brightness (LSB) galaxies have shown that the range of surface brightness covered in traditional, "magnitude-limited" redshift surveys is limited (Sprayberry *et al.* 1997). However, Sprayberry *et al.* also showed that the vast majority of galaxies overlooked in surveys like the SSRS2 are intrinsically faint (see their Figure 4). The contribution of LSBs to the galaxy density at L_* is less than 10%. Because the galaxy counts are largely determined by galaxies near L_*, (unless the luminosity function of LSBs is much steeper than observed), the bias against LSBs is unlikely to affect the counts significantly. At L_*, we therefore expect the combined errors from galaxy detection and star/galaxy separation to be smaller than 20%.

If the steep slope cannot be blamed on errors in detection or photometry, then the next most plausible alternatives are recent evolution in the galaxy population or large-scale density fluctuations. Both of these options have been constrained somewhat by recent redshift surveys. Ellis *et al.* (1996) have shown that the space density of galaxies derived from the Autofib redshift survey is a factor of two larger than we derive from the SSRS2 in the redshift range $0 \leq z \leq 0.1$. However, it is important to point out that most galaxies used in their computation lie near the upper limit of the redshift bin, $z = 0.1$. Furthermore, Ellis *et al.* eliminated the DARS (Peterson *et al.* 1986) from the analysis of the Autofib survey when they concluded that the space density

of galaxies in this sample was anomalously low. The magnitude limit of the DARS is $B = 17$, comparable to other surveys finding low normalizations. The exclusion of the DARS was well justified: because Ellis *et al.* (1996) computed the LF using a technique that is biased by density fluctuations, they recognized that the *shape* of the LF computed from the combined (bright+faint) samples would be biased if the overall densities in the individual samples were significantly different. However, the elimination of low-redshift, low-normalization regions clearly biases the determination of the overall normalization at $z \leq 0.1$.

Using the field complement of the Norris Survey, Small, Sargent and Hamilton (1997) also measure a large space density (similar to Autofib) at $z \leq 0.2$. In this case, the mean redshift of the low-redshift sample is $z = 0.15$, and once again the survey is essentially disjoint from the SSRS2, the Stromlo-APM, and other low-normalization surveys. The Century Survey (Geller *et al.* 1997), which samples the entire region $z \leq 0.15$, yields evidence of a 50% increase in the normalization at $z \geq 0.06$. Geller *et al.* note that errors in the selection function may mimic such an increase, and they interpret their data cautiously. Taken together, however, these surveys provide constraints on the timescale (or alternatively the spatial scale) over which the normalization would have to change. The luminosity function appears relatively stable between $z = 0.2$ and $z = 0.1$ and then drops rapidly at lower redshift. In order to match the density field measured from the low-redshift surveys, the change must be remarkably abrupt; these surveys indicate little change in the density at $z \leq 0.1$ (*e.g.*, Loveday *et al.* 1992, Ratcliffe *et al.* 1998). Such a discontinuity seems very unlikely to be an evolutionary effect, especially given that the galaxy counts in the K-band show a similar trend (Huang *et al.* 1996, but see Bertin & Dennefeld 1997*b* for a dissenting view). Unless there are large, systematic errors swaying all of the low-redshift surveys in the same direction, then the most likely explanation is that a very large portion of the southern sky (at least $150h^{-1}$ Mpc across) is underdense by approximately a factor of two.

If a local hole is the source of the anomalously steep galaxy counts, then it must be remarkably uniform over the region covered by the SSRS2. We see no evidence of substantial density gradients from one part of the survey to another. Figure 8 shows a comparison between the SSRS2 subsamples in the northern and southern Galactic hemispheres. In this figure, we show the redshift distribution for each subsample along with the predictions based on a single luminosity function computed from the entire SSRS2. The solid curve in panels *a*, *c* and *e* represents the expected redshift distribution for a uniform distribution of galaxies in space. Each curve is scaled only by the solid angle of the subsample. Large-scale structure is clearly evident in each panel; however, the overall density of galaxies is remarkably constant from one section of the survey to the other. To check this, we have also fitted luminosity functions to each subsample independently. The luminosity functions for SSRS2 North and South are consistent at the 1σ level in both shape and normalization, and they are also indistinguishable from the overall SSRS2 luminosity function. This agreement is reflected in the shape and the overall normalization of the redshift distributions in Figure 8. The most extensive feature in either subsample is the underdensity in the north at $z \approx 0.035$. Although this underdense region is quite large, it is still counteracted by the

overdensities at lower redshift in such a way that the overall density of SSRS2 North is consistent with the SSRS2 as a whole.

Figure 8 also shows very little trend in the observed mean density with redshift. Panels *b*, *d* and *f* show the ratio of the observed redshift distribution to the expected distribution, and aside from the well-known fluctuations caused by typical voids and walls, the ratio is remarkably stable. The error bars in this panel have been left out for clarity, but it is important to note that beyond $z = 0.05$, the ratio is highly uncertain (as can be seen from the small number of galaxies in the corresponding panel *a*). Tiny uncertainties in the shape of the luminosity function also contribute to large uncertainties at $z \geq 0.05$. Although there appears to be some hint of a density increase in this redshift range, it is not statistically significant in either subsample or in the SSRS2 as a whole.

According to our current picture of large-scale structure, a local underdensity of the required magnitude and covering such a large volume would be surprising; the *rms* fluctuations computed from the observed power spectrum are only ∼10% on this scale (*e.g.*, Baugh 1996). If density fluctuations are Gaussian, then the probability of observing a factor of two underdensity in our own backyard seems disturbingly small. However, recent progress in our understanding of large-scale structure has been punctuated by a few notable surprises (*e.g.*, de Lapparent, Geller & Huchra 1986, Davis *et al.* 1982), and it seems premature to dismiss the possibility of very large-scale structure on this basis alone. Recent observations suggest that such large density fluctuations may not be so rare: the Corona Borealis region, for example, exceeds the mean galaxy density by ∼70% on scales of $100h^{-1}$ Mpc (Geller *et al.* 1997). Even a glance at the LCRS redshift distribution suggests that at least some modulation of the density on these very large scales is common. More quantitatively, Landy *et al.* (1996) have found excess power in the two-dimensional power spectrum at $\sim 100h^{-1}$ Mpc. It remains to be seen whether the frequency of such large-scale features is large enough to remove the novelty of the putative local hole. Surveys covering larger volumes will be necessary to resolve this question definitively.

In an attempt to be as faithful to the entire range of observations as possible, we create a fiducial no-evolution model for the galaxy counts which accounts for a low-redshift change in the normalization. We form this prediction by assuming that the shape of the LF does not evolve but that the density increases smoothly over the redshift range $0.08 \leq z \leq 0.12$. Some justification of this assumption can be found in the LCRS, which covers the entire region $0 \leq z \leq 0.2$. In Figure 8 of Lin *et al.* (1996), there is some evidence of a discontinuity in the density field at approximately $z = 0.07$. The magnitude of the observed jump falls short of the required factor of 2.3, but the volume in this region of the LCRS is quite small. We have arbitrarily chosen a smooth function to bridge the gap between the low-normalization and high-normalization regions: $\phi_*(z) = \phi_*(z < 0.05)f(z)$ where $f(z) = 1 + \{\exp[-(z - z_c)/\Delta z] + 1\}^{-1}$ with $z_c = 0.1$ and $\Delta z = 0.01$. This fiducial model of the total galaxy counts is shown as the dashed line in Figure 7 and is roughly consistent with the galaxy counts to $B \sim 20$.

5.2. The Faint End of the E/S0 LF

The spectacular progress in our ability to discern faint-galaxy morphology has inspired a re-evaluation of the faint end of the local E/S0 luminosity function. As we noted in §4, the best available estimates of the field E/S0 LF are strongly contradictory. Loveday *et al.* (1992) found a steeply decreasing faint end in the Stromlo-APM survey ($\alpha = +0.2 \pm 0.35$), while Marzke *et al.* (1994*a*) found a flat faint end ($\alpha = -0.97 \pm 0.2$) in the CfA survey. Both Marzke *et al.* (1994*a*) and Zucca *et al.* (1994) showed that incompleteness in the Stromlo-APM survey could be responsible for the steeply declining faint end. Because only 1310 of the 1658 Stromlo-APM galaxies were morphologically classified, Marzke *et al.* (1994*a*) suggested that the correlation between intrinsic luminosity and classifiability (essentially apparent size in this case) could have caused a bias against intrinsically faint, early-type galaxies. Monte Carlo simulations showed that the bias was sufficient to cause the observed discrepancy in the LF and also to account for the anomalously low V/V_{max} obtained for this sample. Because of the uncertainty in both the Stromlo-APM LF and the CfA LF, the true abundance of faint, local E/S0's has remained a nagging question.

With the arrival of the HST Medium Deep Survey (Griffiths *et al.* 1994,ApJ,437,67) and the Hubble Deep Field (Williams *et al.* 1996), the possibility of a flat E/S0 LF gained new popularity. Glazebrook *et al.* (1995) and Driver *et al.* (1995*b*) showed that a flat E/S0 LF combined with a high overall normalization produced no-evolution predictions which very nearly matched the E/S0 counts from the HST Medium Deep Survey. Driver *et al.* (1995*a*) drew similar conclusions from a very deep HST field near a high-redshift radio galaxy, and Abraham *et al.* (1996) used the HDF counts to follow the trend to $I = 25$. As we discussed in §5.1, the case for a high normalization at modest redshifts has been strengthened by the results of the Autofib, Norris and Century redshift surveys. However, the choice of $\alpha \approx 1$, which is critical to the conclusion that early-types follow the no-evolution predictions, has remained somewhat arbitrary.

Because it combines the advantages of the Stromlo-APM and the CfA surveys, the SSRS2 is uniquely capable of improving this measurement. Like the Stromlo survey, the SSRS2 is based on a well-calibrated and reproducible photometric catalog. On the other hand, the SSRS2 targets nearby (and therefore apparently large) galaxies and thus allows more detailed galaxy classification. Like the CfA survey, morphological classification in the SSRS2 is more than 99% complete. The flat faint-end slope measured for early-types in the SSRS2 lends strong support to the conclusions of Driver *et al.* (1995*a*, *b*), Glazebrook *et al.* (1995) and Abraham *et al.* (1996) regarding the counts of faint Es and S0s. In order to provide a useful benchmark, we have computed no-evolution models based on our measured LFs and recorded them in Tables 3 and 4. These models include the redshift-dependent ϕ_* discussed in §5.1 and type-dependent K-corrections based on the Rocca-Volmerange & Guiderdoni (1988) models. We compute $N(m)$ in B and then in I_{814} using a mean color for each type from Windhorst *et al.* (1994): $\langle B - I \rangle$ = 2.3, 1.9 and 1.4 for E/S0s, spirals and irregulars, respectively. We include models for two values of the deceleration parameter: for each type, the first column represents $q_0 = 0.5$ while the second column represents $q_0 = 0.05$. The values listed in the tables are raw galaxy counts *before*

convolution with a magnitude-error distribution.

Figure 9 compares the HDF counts with the I-band no-evolution models. These models, which are intended to represent the most objective possible interpretation of both the low-z and intermediate-z redshift surveys, reproduce the E/S0 counts very well. Indeed, given that stars in these galaxies obviously evolve with time, the agreement is almost *too* good; one expects passive luminosity evolution to produce at least some enhancement in the counts at faint magnitudes unless it is counteracted by a decrease in number density. Ongoing studies of the colors and redshift distributions of these faint early-types should help to disentangle these competing effects.

Although the case for a flat E/S0 LF now seems quite convincing, the connection to other LFs based on spectral type and color remains somewhat puzzling. For example, Lin *et al.* (1996) have shown that galaxies with weak OII emission have a steeply declining LF ($\alpha = -0.3 \pm 0.1$) at magnitudes fainter than M_*. Given the correlation between star-formation and morphology, this seems surprising; one expects the weak-OII LF to reproduce the E/S0 LF at least to first order. A more detailed analysis of the LCRS confirms the dependence of the LF on spectral type and shows a continuous variation from a steeply declining LF for the earliest spectral types to steeply increasing LFs for star-forming galaxies (Bromley *et al.* 1997). A similar picture emerges from the dependence of the SSRS2 LF on color: the LF of red galaxies in the SSRS2 declines somewhat at the faint end ($\alpha = -0.73 \pm 0.24$) while the blue galaxy LF is relatively steep ($\alpha = -1.46 \pm 0.18$, Marzke & da Costa 1997). The fact that the color dependence mimics the dependence on emission strength seems reasonable: both are strongly tied to recent star formation, while the processes governing galaxy morphology are less clear. The large scatter in the relations between color and morphology and between line strength and morphology may hide strong luminosity dependencies, which in themselves would provide interesting constraints on galaxy formation. Samples large enough (and homogeneous enough) to determine the full multivariate distribution in luminosity, color, morphology and spectral type will clearly provide a major step forward in our understanding of galaxy formation.

As a final note, we emphasize that we do not distinguish in this paper between the various classes of spheroidal galaxies. Dwarf spheroidals, giant ellipticals and lenticular galaxies all fall into our E/S0 bin. Using these coarse morphologies alone, we obviously cannot comment on the LFs of more specific classes of galaxies. For example, the very detailed morphological decomposition of the Virgo cluster luminosity function (Sandage, Binggeli & Tammann 1985) reveals a series of roughly Gaussian type-specific luminosity functions with varying central magnitudes; only the dEs are unbounded at the faint end (to the limit of the survey, at least). Upon closer examination, the field E/S0 LF may reveal a similar construction. One of us is currently obtaining CCD imaging of faint SSRS2 galaxies to explore this possibility further.

5.3. The Shape of the Irregular/Peculiar LF

The remarkable increase in irregular morphology at faint apparent magnitudes reported by Driver *et al.* (1995*a*, *b*), Glazebrook *et al.* (1995) and Abraham *et al.* (1996) raises two related questions: first, what fraction of these faint irregular galaxies are simply nearby dwarfs? Second, if the majority of these irregulars lie at high redshift, what are their descendents at the present epoch?

Koo, Gronwall & Bruzual (1993) showed that uncertainties in the local luminosity function (particularly at the faint end) play a pivotal role in our interpretation of the faint galaxy counts. If our tally of nearby dwarfs is incomplete, then no-evolution predictions will fall short of the observed galaxy counts even in the absence of real evolution. Marzke, Huchra & Geller (1994*b*) showed that such an underestimate had indeed occurred: at the faint end of the luminosity function, there were more galaxies than would be predicted by the extrapolation of the Schechter function fitted to the bright end. However, the magnitude of the excess was uncertain, and because of the small volume of the universe probed at these faint absolute magnitudes, it remained unclear whether this excess was peculiar to the local region or whether it was a global feature of the present epoch.

Later, Marzke *et al.* (1994*a*) determined that the galaxies responsible for the faint-end excess were very late-type spirals and irregulars. The luminosity function of this class was remarkably steep: $\alpha = -1.88 \pm 0.2$. As we discussed earlier, however, the Zwicky magnitude scale was uncertain, and the overall contribution of these nearby late types to the deep galaxy counts was unclear. The improved photometric scale and the well-defined detection algorithm used in the construction of the SSRS2 allow us to measure the irregular-galaxy LF with much greater confidence. The slope of the Irr/Pec LF we measure here is essentially identical to the slope of the CfA Sm-Im LF: $\alpha = -1.81 \pm 0.24$. Although the random error associated with the new measurement is comparable to the older CfA measurements, the systematic uncertainties, which were difficult to quantify in the CfA, are certainly reduced in the SSRS2. Nevertheless, Figure 6 shows that the faint end of the Irr/Pec LF reproduces the CfA Sm-Im LF very well. As noted in §4, the differences between the two LFs occur at the bright end.

As with the CfA survey, however, the volume surveyed at the faintest absolute magnitudes is still quite small, and if the shape of the Irr/Pec LF depends on the particular details of the very nearby universe, then it may be unwise to extrapolate this result to the faint galaxy counts. However, several recent observations suggest that the steep Irr/Pec LF is not a local oddity. Bromley *et al.* (1997) have shown that the class of LCRS galaxies exhibiting the most active star formation (according to their spectral energy distributions) have a very steep luminosity function: $\alpha = -1.93 \pm 0.13$. Although the LCRS sample does not have detailed morphological classifications, the fact that essentially all irregular galaxies show strong emission lines suggests that these LFs represent the same class of galaxies. Although the LCRS LFs do not extend as faint as the CfA or SSRS2, their redshift range is much greater, and the possibility that the steep LF is a local fluke

seems less likely.

Another related observation is the recent UV-selected survey of Treyer *et al.* (1996). This survey of ~ 40 galaxies covers the redshift range $0 \leq z \leq 0.3$ and is selected by $2000\mathring{A}$ flux. Because of the huge variation in $m_{2000} - B$ across the Hubble sequence, this sample is dominated by late-type, star-forming galaxies. Although the sample is small, Treyer *et al.* were able to show that the faint-end slope of the LF is steep: $\alpha = -1.77 \pm 0.15$, clearly consistent with the Irr/Pec LF measured here, the LF of star-forming galaxies measured by Bromley *et al.* (1997), the luminosity function of the bluest quartile in the SSRS2 ($\alpha \approx -1.7$, Marzke & da Costa 1997) and the Sm-Im LF of the CfA survey (Marzke *et al.* 1994). It is also worth noting that the observed HI mass function of gas-rich galaxies is not inconsistent with an upturn at the low-mass end; the distribution is still poorly determined in this regime (Schneider 1997, Zwaan *et al.* 1997). Given the growing consensus, it now seems reasonable to conclude that the steep luminosity function is a universal feature of star-forming galaxies.

The last panel in Figure 9 shows the HDF counts of irregulars and peculiars along with the no-evolution predictions described in §5.2. Although our models differ in detail with the earlier models from Driver *et al.* (1995a, b), Glazebrook *et al.* (1995) and Abraham *et al.* (1996), the excess of faint irregulars is so pronounced that the overall conclusion remains unchanged: the no-evolution models cannot account for the irregular population at faint magnitudes. It appears very unlikely that remaining uncertainties in the local luminosity function will be able to make up the difference. For example, the two sets of curves represent different assumptions about the behavior of the LF at fainter luminosities than we can measure from the SSRS2: the lower curve represents a cutoff at $M_B = -14$, the limit of our survey, while the upper curve extrapolates the steep LF all the way to $M_B = -10$. The extrapolation makes very little difference.

More detailed information about the faint irregular population is slowly becoming available. Perhaps the most robust conclusion that can be drawn from a comparison of our local survey to the results of the deep redshift surveys (Brinchman *et al.* 1997, Lilly *et al.* 1997) is that the super-L_* irregulars observed by Brinchman *et al.* (1997) and Glazebrook *et al.* (1997) at redshifts greater than a half have very few local counterparts. For example, the density of galaxies at $M \approx -21$ is more than an order of magnitude higher at $z \geq 0.75$ than it is locally. Brinchman *et al.* drew a similar conclusion from their own data, which yielded no super-L_* irregulars at $z \leq 0.5$ even though they could have been detected had they been present in the numbers observed at higher redshift. With larger, more homogeneous surveys planned for the near future, the relationship between the bright irregulars at high redshift and their faint, low-redshift counterparts should soon become more clear.

6. Conclusions

We have used a new sample of 5,404 galaxies with rough but complete morphological classifications to determine the galaxy luminosity function for different morphologies over the range $-22 \leq M_B \leq -14$. We conclude that the faint-end slope for both E/S0 and spiral galaxies is essentially flat over this range. The LF of irregular and peculiar galaxies is very steep ($M_* - 19.78^{+0.40}_{-0.50} + 5\log h$, $\alpha = 1.81^{+0.24}_{-0.24}$, $\phi_* = 0.2 \pm 0.08 \times 10^{-3} h^3\,\mathrm{Mpc}^{-3}$). The faint-end slope of the Irr/Pec LF is consistent with earlier measurements from the CfA Redshift Survey, however, an excess of bright irregulars relative to the CfA LF leads to a brighter value of M_* for this class in the SSRS2. This pattern appears in each morphological class and may be evidence that bright galaxies are generally underrepresented in the CfA Survey.

The flat faint-end slope of the E/S0 LF supports earlier claims that the Stromlo-APM LF under-represents faint early-type galaxies. As a result, the no-evolution predictions of faint E/S0 counts based on the SSRS2 exceed the predictions based on the Stromlo-APM and, assuming that the high normalization obtained for the intermediate-redshift LFs is representative, the SSRS2 predictions are consistent with the observed counts of Es and S0s to $I = 25$. As with other surveys to similar depths, however, the normalization obtained directly from the SSRS2 is low, and the explanation of this low-redshift anomaly remains elusive. Until the biases in the present-epoch luminosity function are better understood, the degree of evolution inferred from deep counts will remain uncertain.

We thank Todd Small, Huan Lin, Julianne Dalcanton, Rebecca Bernstein, Elena Zucca and Richard Ellis for helpful discussions. We also thank Seth Cohen for his help with Figure 7 and an anonymous referee for stimulating a more lengthy version of §5.

TABLE 1

Schechter Function Parameters
$-22 \leq M_B \leq -13.5$

	Sample	N_{gal}	M_*	α	$\phi_*(10^{-3}\,\mathrm{Mpc}^{-3})$	$P(\ln \mathcal{L}_1/\mathcal{L}_2)$
	All	5036	$-19.43^{+0.06}_{-0.06}$	$-1.12^{+0.05}_{-0.05}$	12.8±2.0	0.03
	E/S0	1587	$-19.37^{+0.10}_{-0.11}$	$-1.00^{+0.09}_{-0.09}$	4.4±0.8	0.04
	Spirals	3227	$-19.43^{+0.08}_{-0.08}$	$-1.11^{+0.07}_{-0.06}$	8.0±1.4	0.03
	Irr/Pec	204	$-19.78^{+0.40}_{-0.50}$	$-1.81^{+0.24}_{-0.24}$	0.2±0.08	0.16
	All	5054	$-19.40^{+0.06}_{-0.06}$	$-1.08^{+0.06}_{-0.05}$	13.7±1.9	0.02
Case 1 Infall	E/S0	1592	$-19.38^{+0.10}_{-0.11}$	$-0.99^{+0.10}_{-0.09}$	4.5±0.9	0.03
	Spirals	3240	$-19.38^{+0.08}_{-0.08}$	$-1.06^{+0.07}_{-0.07}$	8.8±1.2	0.02
	Irr/Pec	204	$-19.69^{+0.39}_{-0.48}$	$-1.74^{+0.25}_{-0.25}$	0.2±0.1	0.09
	All	5060	$-19.41^{+0.06}_{-0.06}$	$-1.09^{+0.06}_{-0.05}$	13.5±1.9	0.02
Case 2 Infall	E/S0	1595	$-19.37^{+0.10}_{-0.11}$	$-1.00^{+0.10}_{-0.09}$	4.5±0.9	0.02
	Spirals	3243	$-19.38^{+0.07}_{-0.08}$	$-1.06^{+0.07}_{-0.07}$	8.7±1.2	0.03
	Irr/Pec	204	$-19.74^{+0.40}_{-0.49}$	$-1.79^{+0.24}_{-0.25}$	0.2±0.1	0.06

TABLE 2

SWML Luminosity Functions
(log number $\mathrm{Mpc}^{-3}\,\mathrm{mag}^{-1}$)

	All		E/S0		Spirals		Irr/Pec	
Magnitude	N	$\phi(M)$	N	$\phi(M)$	N	$\phi(M)$	N	$\phi(M)$
-21.10	239	$-3.60^{+0.03}_{-0.03}$	75	$-4.12^{+0.05}_{-0.05}$	157	$-3.79^{+0.03}_{-0.04}$	7	$-5.23^{+0.15}_{-0.23}$
-20.32	1208	$-2.78^{+0.01}_{-0.01}$	387	$-3.27^{+0.02}_{-0.02}$	785	$-2.98^{+0.02}_{-0.02}$	32	$-4.47^{+0.09}_{-0.12}$
-19.53	1525	$-2.31^{+0.01}_{-0.01}$	493	$-2.79^{+0.02}_{-0.02}$	978	$-2.53^{+0.01}_{-0.01}$	51	$-3.91^{+0.08}_{-0.09}$
-18.74	1007	$-2.07^{+0.02}_{-0.02}$	320	$-2.58^{+0.03}_{-0.03}$	655	$-2.27^{+0.02}_{-0.02}$	28	$-3.65^{+0.09}_{-0.11}$
-17.94	517	$-1.91^{+0.02}_{-0.02}$	161	$-2.42^{+0.04}_{-0.04}$	316	$-2.15^{+0.03}_{-0.03}$	36	$-2.98^{+0.08}_{-0.10}$
-17.16	237	$-1.86^{+0.03}_{-0.04}$	67	$-2.43^{+0.06}_{-0.07}$	153	$-2.07^{+0.04}_{-0.05}$	17	$-2.84^{+0.12}_{-0.16}$
-16.36	174	$-1.71^{+0.04}_{-0.04}$	47	$-2.33^{+0.07}_{-0.09}$	108	$-1.92^{+0.05}_{-0.06}$	18	$-2.52^{+0.13}_{-0.18}$
-15.58	83	$-1.70^{+0.05}_{-0.06}$	26	$-2.31^{+0.09}_{-0.11}$	46	$-1.94^{+0.07}_{-0.08}$	9	$-2.48^{+0.16}_{-0.25}$
-14.78	23	$-1.55^{+0.09}_{-0.12}$	6	$-2.35^{+0.16}_{-0.26}$	14	$-1.68^{+0.12}_{-0.16}$	3	$-2.17^{+0.24}_{-0.58}$
-14.00	10	$-1.18^{+0.14}_{-0.21}$	1	$-2.30^{+0.31}_{-\infty}$	6	$-1.36^{+0.18}_{-0.30}$	3	$-1.40^{+0.30}_{-1.63}$

TABLE 3

B-band No-evolution Models with a Local Hole
(log counts deg^{-2} mag^{-1})

B	All		E/S0		Spiral		Irr/Pec	
10.5	-2.86	-2.86	-3.36	-3.36	-3.06	-3.06	-4.28	-4.28
11.0	-2.56	-2.56	-3.06	-3.06	-2.77	-2.77	-3.98	-3.98
11.5	-2.27	-2.27	-2.77	-2.77	-2.47	-2.47	-3.68	-3.68
12.0	-1.97	-1.97	-2.48	-2.48	-2.18	-2.18	-3.38	-3.38
12.5	-1.68	-1.68	-2.19	-2.19	-1.89	-1.89	-3.09	-3.09
13.0	-1.39	-1.39	-1.90	-1.90	-1.60	-1.60	-2.79	-2.79
13.5	-1.10	-1.10	-1.61	-1.61	-1.31	-1.31	-2.50	-2.50
14.0	-0.82	-0.82	-1.33	-1.33	-1.02	-1.02	-2.20	-2.20
14.5	-0.54	-0.54	-1.05	-1.05	-0.74	-0.74	-1.91	-1.91
15.0	-0.26	-0.26	-0.77	-0.77	-0.47	-0.47	-1.63	-1.63
15.5	0.01	0.01	-0.50	-0.50	-0.20	-0.19	-1.34	-1.34
16.0	0.28	0.28	-0.24	-0.24	0.07	0.07	-1.06	-1.06
16.5	0.54	0.54	0.02	0.02	0.33	0.33	-0.78	-0.78
17.0	0.80	0.80	0.28	0.28	0.59	0.60	-0.50	-0.50
17.5	1.07	1.07	0.54	0.55	0.87	0.87	-0.21	-0.21
18.0	1.35	1.35	0.82	0.82	1.15	1.15	0.08	0.08
18.5	1.62	1.63	1.09	1.10	1.42	1.42	0.36	0.37
19.0	1.88	1.89	1.35	1.36	1.68	1.68	0.64	0.64
19.5	2.12	2.13	1.58	1.60	1.91	1.93	0.91	0.91
20.0	2.34	2.36	1.80	1.82	2.13	2.15	1.16	1.17
20.5	2.55	2.57	2.00	2.02	2.34	2.36	1.41	1.42
21.0	2.74	2.76	2.18	2.21	2.53	2.56	1.65	1.67
21.5	2.92	2.95	2.35	2.38	2.71	2.74	1.89	1.90
22.0	3.09	3.13	2.51	2.55	2.88	2.92	2.12	2.14
22.5	3.25	3.29	2.65	2.70	3.04	3.09	2.35	2.37
23.0	3.40	3.45	2.79	2.85	3.19	3.24	2.58	2.60
23.5	3.55	3.61	2.91	2.98	3.34	3.40	2.80	2.82
24.0	3.70	3.76	3.02	3.10	3.49	3.55	3.02	3.05
24.5	3.87	3.92	3.13	3.22	3.66	3.71	3.23	3.27
25.0	4.04	4.09	3.24	3.33	3.83	3.88	3.43	3.48
25.5	4.22	4.27	3.35	3.44	4.01	4.06	3.62	3.69
26.0	4.39	4.46	3.46	3.56	4.18	4.25	3.80	3.89
26.5	4.55	4.65	3.60	3.69	4.34	4.44	3.97	4.08
27.0	4.67	4.83	3.74	3.83	4.46	4.62	4.14	4.26
27.5	4.76	4.99	3.89	3.98	4.55	4.78	4.30	4.43
28.0	4.83	5.12	4.03	4.15	4.62	4.91	4.46	4.60
28.5	4.89	5.22	4.13	4.32	4.67	5.01	4.61	4.75
29.0	4.93	5.30	4.21	4.47	4.71	5.09	4.75	4.91

TABLE 4

I-band No-evolution Models with a Local Hole
(log counts deg^{-2} mag^{-1})

I_{814}	All		E/S0		Spiral		Irr/Pec	
10.5	-1.72	-1.72	-1.98	-1.98	-1.92	-1.92	-3.43	-3.43
11.0	-1.42	-1.42	-1.69	-1.69	-1.63	-1.63	-3.13	-3.13
11.5	-1.13	-1.13	-1.39	-1.39	-1.33	-1.33	-2.84	-2.84
12.0	-0.84	-0.84	-1.10	-1.10	-1.04	-1.04	-2.54	-2.54
12.5	-0.55	-0.55	-0.81	-0.81	-0.75	-0.75	-2.24	-2.24
13.0	-0.26	-0.26	-0.53	-0.53	-0.46	-0.46	-1.95	-1.95
13.5	0.03	0.03	-0.25	-0.24	-0.18	-0.18	-1.65	-1.65
14.0	0.31	0.31	0.04	0.04	0.11	0.11	-1.36	-1.36
14.5	0.60	0.60	0.34	0.34	0.39	0.39	-1.07	-1.07
15.0	0.89	0.89	0.65	0.65	0.69	0.69	-0.77	-0.77
15.5	1.21	1.21	0.97	0.97	1.00	1.00	-0.46	-0.46
16.0	1.52	1.52	1.28	1.28	1.32	1.32	-0.15	-0.15
16.5	1.83	1.83	1.57	1.57	1.62	1.62	0.17	0.17
17.0	2.11	2.12	1.83	1.84	1.90	1.91	0.49	0.49
17.5	2.37	2.38	2.07	2.08	2.16	2.17	0.79	0.79
18.0	2.61	2.62	2.29	2.31	2.40	2.42	1.08	1.08
18.5	2.83	2.85	2.50	2.53	2.63	2.65	1.36	1.37
19.0	3.04	3.07	2.69	2.72	2.84	2.86	1.63	1.63
19.5	3.23	3.27	2.86	2.91	3.03	3.06	1.88	1.89
20.0	3.41	3.46	3.02	3.08	3.21	3.25	2.12	2.14
20.5	3.58	3.63	3.16	3.24	3.37	3.43	2.36	2.38
21.0	3.72	3.80	3.29	3.38	3.52	3.59	2.58	2.61
21.5	3.86	3.94	3.40	3.51	3.65	3.73	2.78	2.83
22.0	3.98	4.08	3.50	3.62	3.77	3.87	2.98	3.03
22.5	4.09	4.20	3.59	3.73	3.87	3.99	3.18	3.23
23.0	4.18	4.32	3.67	3.82	3.97	4.10	3.36	3.42
23.5	4.28	4.42	3.75	3.92	4.07	4.21	3.55	3.61
24.0	4.37	4.52	3.82	4.00	4.15	4.31	3.73	3.80
24.5	4.45	4.62	3.88	4.09	4.24	4.41	3.90	3.98
25.0	4.53	4.72	3.94	4.16	4.32	4.50	4.07	4.16
25.5	4.62	4.81	4.00	4.24	4.40	4.59	4.24	4.34
26.0	4.70	4.90	4.06	4.31	4.48	4.68	4.41	4.51
26.5	4.78	5.00	4.11	4.38	4.56	4.78	4.57	4.68
27.0	4.84	5.10	4.17	4.44	4.63	4.88	4.73	4.84
27.5	4.90	5.19	4.22	4.51	4.68	4.97	4.88	5.00
28.0	4.95	5.27	4.26	4.58	4.73	5.06	5.03	5.15
28.5	4.99	5.34	4.29	4.65	4.76	5.12	5.17	5.30
29.0	5.02	5.39	4.31	4.71	4.80	5.18	5.31	5.45

REFERENCES

Abraham, R.G., Tanvir, N.R., Santiago, B.X., Ellis, R.S., Glazebrook, K., & van den Bergh, S., 1996 MNRAS, 279, L47

Alonso, M. V., da Costa, L. N., Pellegrini, P. S., & Kurtz, M. J. 1993, AJ, 106, 676

Alonso, M. V., da Costa, L. N., Latham, D. W., Pellegrini, P. S., & Milone, A. E. 1994, AJ, 108, 1987

Baugh, C. 1996, MNRAS, 282, 1413

Bertin, E. & Dennefeld, M. 1997*a* A&A, 317, 43

Bertin, E. & Dennefeld, M. 1997*b* A&A, 323, 685

Brinchmann, J., Abraham, R., Schade, D., Tresse, L., Ellis, R.S., Lilly, S.J., Le Fevre, O., Glazebrook, K., Hammer, F., Colless, M., Crampton, D. & Broadhurst, T. 1997, astro-ph #9712060

Bromley, B.C., Press, W.H., Lin, H., & Kirshner, R.P. 1997, astro-ph # 9711227

Burstein, D., & Heiles, C. 1982 AJ, 87, 1165

Corwin, H.G., de Vaucouleurs, A., & de Vaucouleurs, G.H., 1985, Southern Galaxy Catalogue, University of Texas Monograph, Astron.,4,1

da Costa, L. N., Geller, M. J., Pellegrini, P. S., Latham, D. W., Fairall, A. P., Marzke, R. O., Willmer, C. N. A., Huchra, J. P., Calderon, J. H., Ramella, M. & Kurtz, M. J., 1994, ApJ Letters, 424, L1

da Costa, L. N., et al. 1997, ApJS in press.

Davis, M., Huchra, J.P., Latham, D.W., & Tonry, J. 1982, ApJ, 253, 423

de Lapparent, V., Geller, M.J. & Huchra, J.P. 1986, ApJ, 302, L1

Dalcanton, J.J., Spergel, D.N. & Summers, 1997 ApJ, 482, 659

Dalcanton, J.J., Spergel, D.N., Gunn, J.E., Schmidt, M., & Schneider, D.P. 1997, astro-ph preprint #9705088

Davis, M. & Huchra, J.P. 1982, ApJ 252, 437

Disney, M.J. 1976, Nature, 263, 573

Driver,S.P., Windhorst, R.A., & Griffiths, R.E. 1995*b* ApJ, 456, L21

Driver,S.P., Windhorst, R.A., Ostrander, E.J., Keel, W.C., Griffiths, R.E., Ratnatunga, K.U. 1995*a*, ApJ, 449, L23

Dressler, A., 1980 ApJ, 236,351

Efstathiou, G., Ellis, R. S., & Peterson, B. A. 1988, MNRAS 232, 431 (EEP)

Ellis, R. S., Colless, M., Broadhurst, T., Heyl, J., & Glazebrook, K. 1996, MNRAS 280, 235

Geller, M.J., Kurtz, M.J., Wegner,G., Thorstensen, J.R., Fabricant,D.G., Marzke, R.O., Huchra, J.P., Schild, R.E. & Falco, E. 1997, AJ, 114, 2205

Glazebrook, K., Ellis, R. S., Colless, M., Broadhurst, T., Allington-Smith, J., & Tanvir, N. 1995, MNRAS 273, 157

Glazebrook, K., Abraham, R., Santiago, B., Ellis, R.S. & Griffiths, R. 1997, astro-ph #9712269

Griffiths *et al.* 1994, ApJ, 437, 67

Gunn, J.E., 1995, BAAS 186,4405

Hashimoto, Y., Oemler, A., Lin, H., Tucker, D.L., astro-ph # 9712319

Heydon-Dumbleton, N.H., Collins, C.A. & MacGillivray, H.T. 1989, MNRAS, 238, 379.

Heyl, J., Colless, M., Ellis, R.S. & Broadhurst, T. 1997 MNRAS, 285, 613

Huchra, J.P. 1976, AJ, 81, 952

Koo, D.C., Gronwall, C. & Bruzual, G.A. 1993, ApJ, 415, 21

Landy, S.D., Shectman, S.A., Lin, H., Kirshner, R.P., Oemler, A. & Tucker, D. 1996, ApJ, 456, L1

Lasker, B. M., Sturch, C. R., McLean, B. M., Russel, J. L., Jenker, H., & Shara, M. 1990, AJ,, 99, 2019 (GSC)

Lauberts, A., & Valentijn, E. A. 1989, The Surface Photometry Catalogue of the ESO/Uppsala Survey,(Garching: ESO)

Lilly, S. J., Tresse, L., Hammer, F. Crampton, D., & Le Fevre, O. 1995, ApJ, 455, 108

Lilly, S.J., Schade, D., Ellis, R.S., Le Fevre, O., Brinchmann, J., Abraham, R., Tresse, L., Hammer, F., Crampton, D., Colless, M., Glazebrook, K., Mallen-Ornelas, G. & Broadhurst, T. 1997, astro-ph #9712061

Lin, H., Kirshner, R. P.,Shectman, S., Landy, S. D., Oemler, A., Tucker, D. L., & Schechter, P. 1996, ApJ, 464, 60

Loveday, J., Peterson, B. A., Efstathiou, G., & Maddox, S. J., 1992, ApJ, 390, 338

Maddox, S., Sutherland, W.J., Efstathiou, G., Loveday, J., & Peterson, B. 1990 MNRAS, 247, 1P.

Maia, M.A.G. & da Costa, L.N. 1990, ApJ, 352,457

Marzke, R. O., & da Costa, L. N. 1997, AJ, 113, 185

Marzke, R. O., Geller, M. J., da Costa, L. N., & Huchra, J. P. 1995, AJ, 110, 477

Marzke, R. O., Geller, M. J., Huchra, J. P., & Corwin, H. G. 1994*a*, AJ 108, 437

Marzke, R. O., Huchra, J. P., & Geller, M. J. 1994*b*, ApJ 428, 43

Metcalfe, N., Fong, R. & Shanks, T. 1995, MNRAS, 274, 769

Metcalfe, N., Shanks, T., Fong, R. & Jones, L.R. 1991, MNRAS, 249, 498

Mo, H.J. , Mao, S. & White, S.D.M. 1998 MNRAS, 295, 319

Odewahn, S.C., Windhorst, R.A., Driver, S.P. & Keel, W.C. 1996, ApJ, 472, L13

Park,C., Vogeley, M.S., Geller, M.J., Huchra, J.P. 1994, ApJ, 431,569

Peterson, B., Ellis, R.S., Efstathiou, G., Shanks, T., Bean, A.J., Fong, R. & Zen-Long,Z., 1986, MNRAS, 221, 233

Postman, M., & Geller, M.J. 1984, ApJ, 281, 95

Ramella, M., Pisani, A., & Geller, M. J. 1997, AJ, 113, 483

Ratcliffe, A., Shanks, T., Parker, Q.A. & Fong, R. 1998, MNRAS 293, 197

Rocca-Volmerange, B. & Guiderdoni, B. 1988, A&AS, 74, 185.

Sandage, A., Tammann, G. A., & Yahil, A. 1979, ApJ 232, 352 (STY)

Sandage, A., Binggeli, B. & Tammann, G.A. 1985, AJ, 90, 1759

Schneider, S.E. 1997, PASA, 14, 99

Small, T.A., Sargent, W.L.W. & Hamilton, D. 1997, ApJ, 487, 512

Sprayberry, D., Impey, C.D., Irwin, M.J., & Bothun, G.D. 1997, ApJ 482, 104

Treyer, M.A., Ellis, R.S., Milliard, B., Donas, J. 1997, astro-ph #9706223

Vorontsov-Velyaminov, B. A., & Arkhipova, V. P. 1963-1968, *The Morphological Catalogue of Galaxies*, (Moscow: Moscow University Press), Parts 2-4 (MCG)

Willmer, da Costa & Pellegrini 1997, astro-ph # 9803118

Williams, R.E. *et al.* 1996, AJ, 112, 1335

Windhorst, R.A., Gordon, J.M., Pascarelle, S.M., Schmidtke, P.C., Keel, W.C., Burkey, J.M. & Dunlop, J.S. 1994, ApJ, 435, 577

Zucca, E., Pozzetti, L. & Zamorani, G. 1994, MNRAS, 269, 953

Zwaan, M.A., Briggs, F.H., Sprayberry, D., & Sorar, E. 1997, ApJ, 490, 173

This preprint was prepared with the AAS LaTeX macros v4.0.

Fig. 1.— A sample of images representing the range of difficulty encountered in galaxy classification. The middle column shows a galaxy of average difficulty in each class, while the left and right columns show approximately the least difficult tenth and the most challenging tenth of the sample, respectively.

Fig. 2.— The dependence of the SSRS2 luminosity function on galaxy morphology. The dashed line connects the SWML estimates for the sample as a whole.

Fig. 3.— Confidence intervals (1σ) on the Schechter shape parameters for different types in the SSRS2.

Fig. 4.— Redshift maps of the SSRS2. The left column includes the entire range of redshifts covered by the survey: $0 \leq cz \leq 20,000$ km s^{-1}. The upper panel shows the southern half of the survey; the lower panel shows the northern half. The panels on the right are enlarged versions of the left-hand panels covering only the redshift range $0 \leq cz \leq 3,000$ km s^{-1}.

Fig. 5.— Luminosity functions for each morphology computed using different assumptions about the local galaxy velocity field. The histogram reproduces the original luminosity functions from Figure 2. The open squares represent case 1 (see text); filled circles represent case 2.

Fig. 6.— A comparison of recent measurements of the LF divided by morphological type. Solid lines and open squares represent the SSRS2; dashed lines represent the CfA Survey and dotted lines represent the Stromlo-APM.

Fig. 7.— A representative compilation of galaxy counts in the B band covering the observed range of apparent magnitudes. Solid triangles indicate the SSRS2, open circles the APM (Maddox *et al.* 1990), triangles the CCD counts of Metcalfe *et al.* (1991), and open squares the Hubble and ASU Deep Fields (Williams *et al.* 1996, Odewahn *et al.* 1996). In each case, magnitudes have been transformed approximately to b_j, which roughly matches the SSRS2 system. The solid line is the fiducial no-evolution model for the galaxy counts based on the shape of the SSRS2 LF but including a normalization which increases by a factor of 2 at $z \sim 0.1$.

Fig. 8.— A comparison of the expected redshift distributions to the measured redshift distributions for subsamples of the SSRS2. From top to bottom, the panels represent the full SSRS2, SSRS2 South, and SSRS2 North. The histograms in the left-hand panels are the observed redshift distributions. The solid lines in these panels are the expectations based on a uniform distribution of galaxies and the overall luminosity function of the SSRS2. The predicted distributions differ only by a scale factor corresponding to the solid angle covered by each subsample; the luminosity function is the same in each panel. The points in the right-hand panels are the ratio of the observed redshift distribution to the predicted one.

Fig. 9.— No-evolution predictions for the Hubble Deep Field galaxy counts from Abraham *et al.* (1996). Solid lines are for $q_0 = 0.05$; dashed lines indicate $q_0 = 0.5$. For the irregulars, two pairs of

lines are shown: the lower pair is computed using a cutoff in the LF at $M_B = -14$. For the upper pair, we extrapolate the Schechter function to $M_B = -10$.

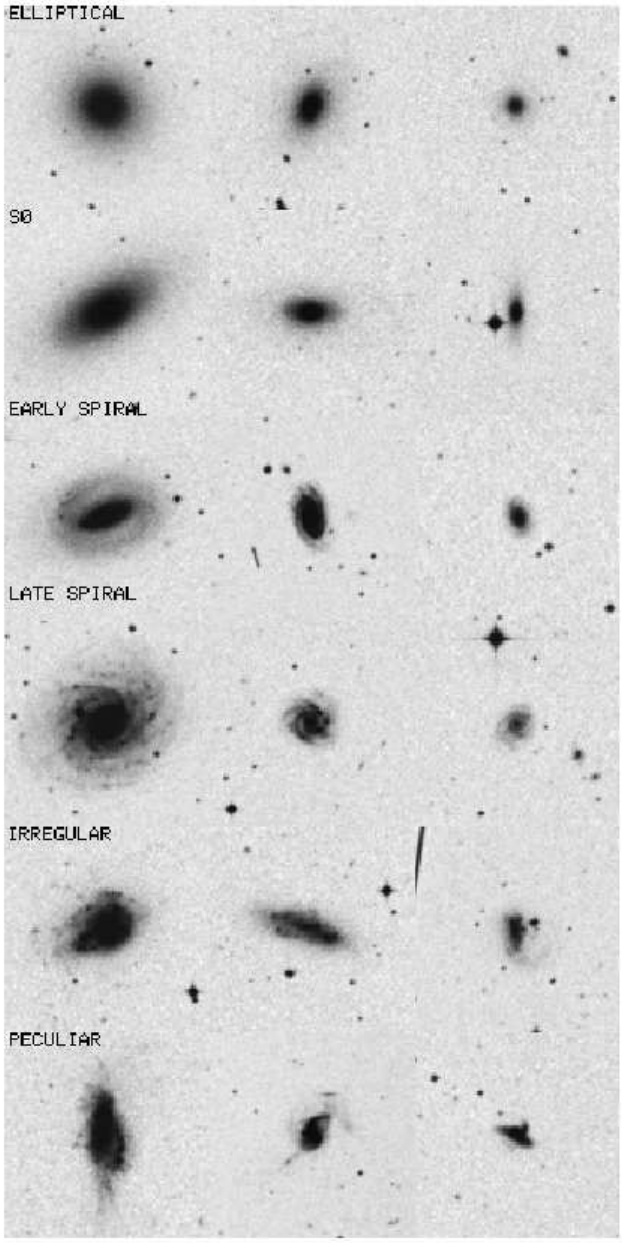
ELLIPTICAL
S0
EARLY SPIRAL
LATE SPIRAL
IRREGULAR
PECULIAR

Figure 1

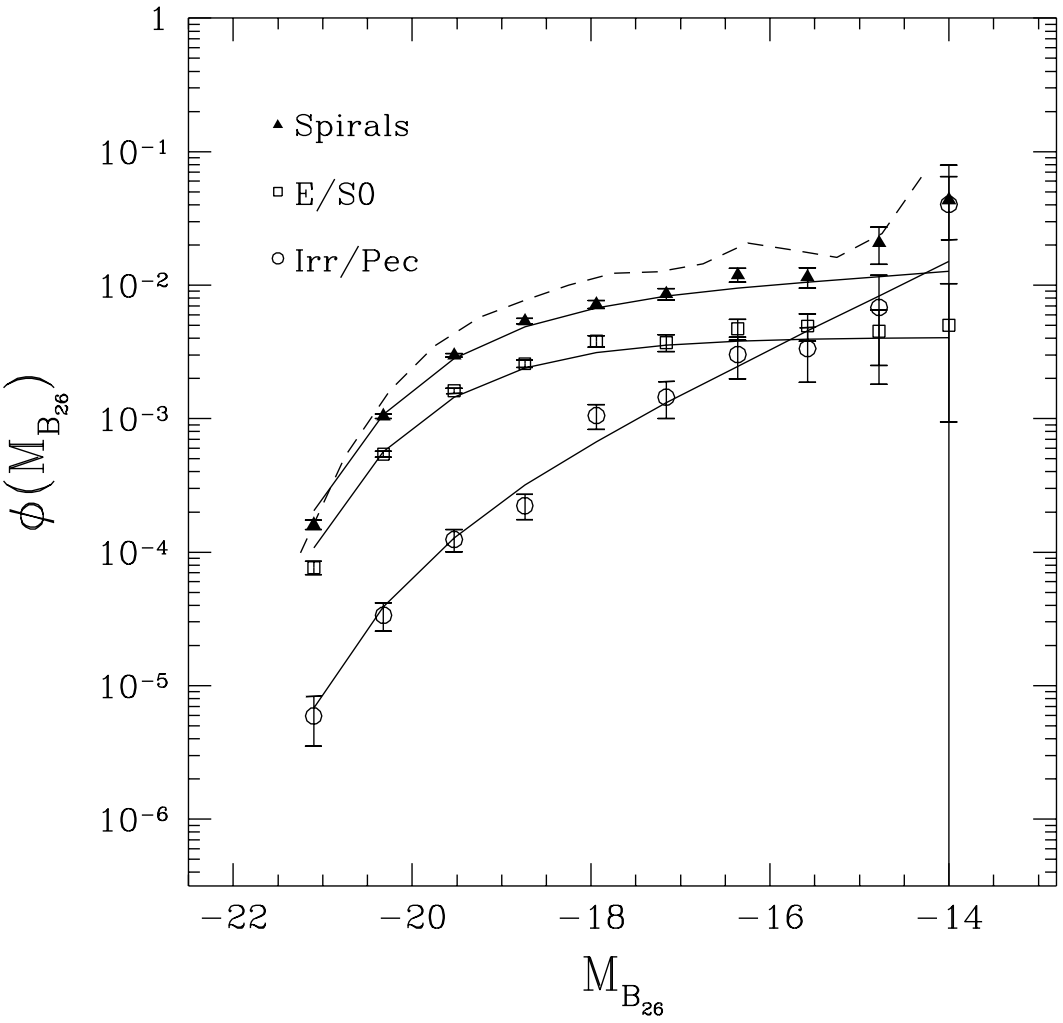
1
10^{-1}
10^{-2}
10^{-3}
10^{-4}
10^{-5}
10^{-6}
$\phi(M_{B_{26}})$
Spirals
E/S0
Irr/Pec
−22
−20
−18
−16
−14
$M_{B_{26}}$

Figure 2

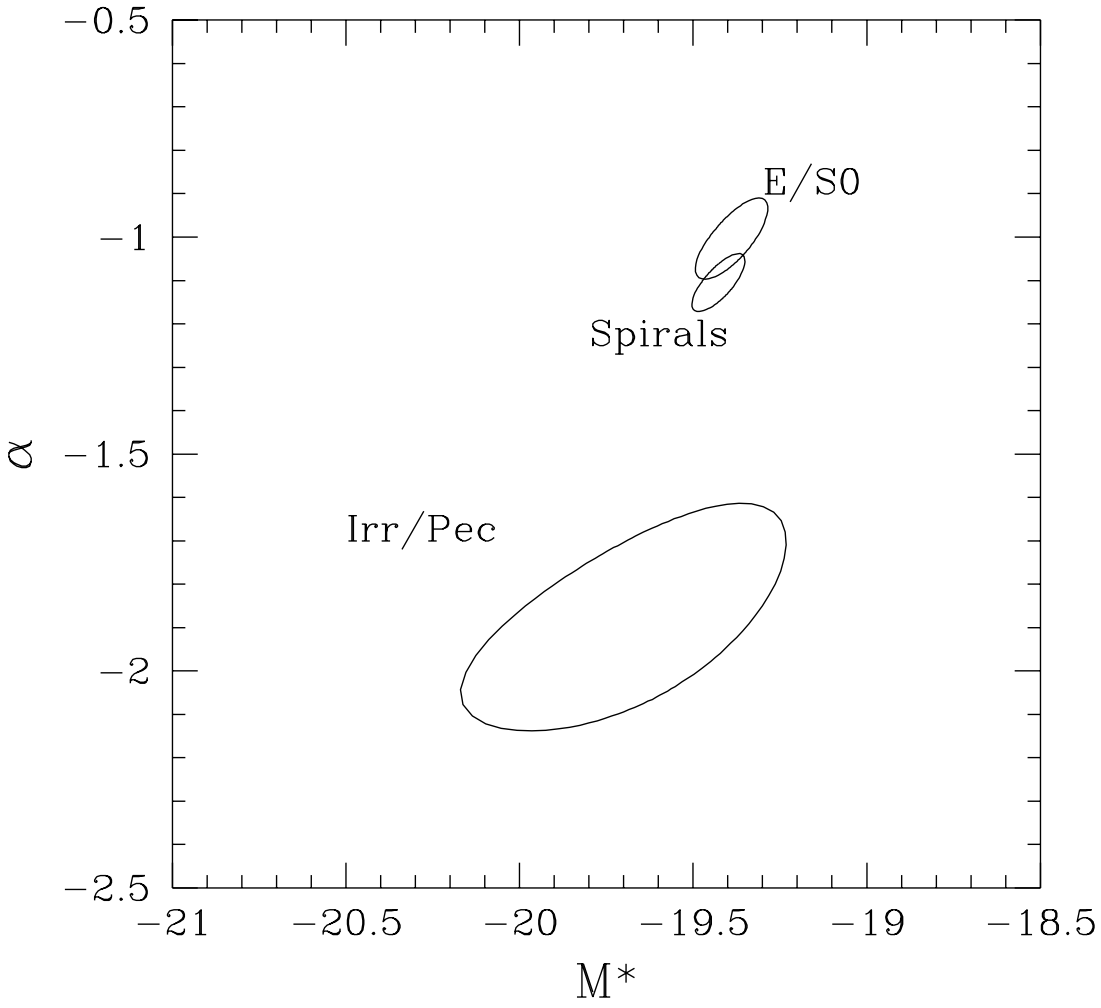

Figure 3

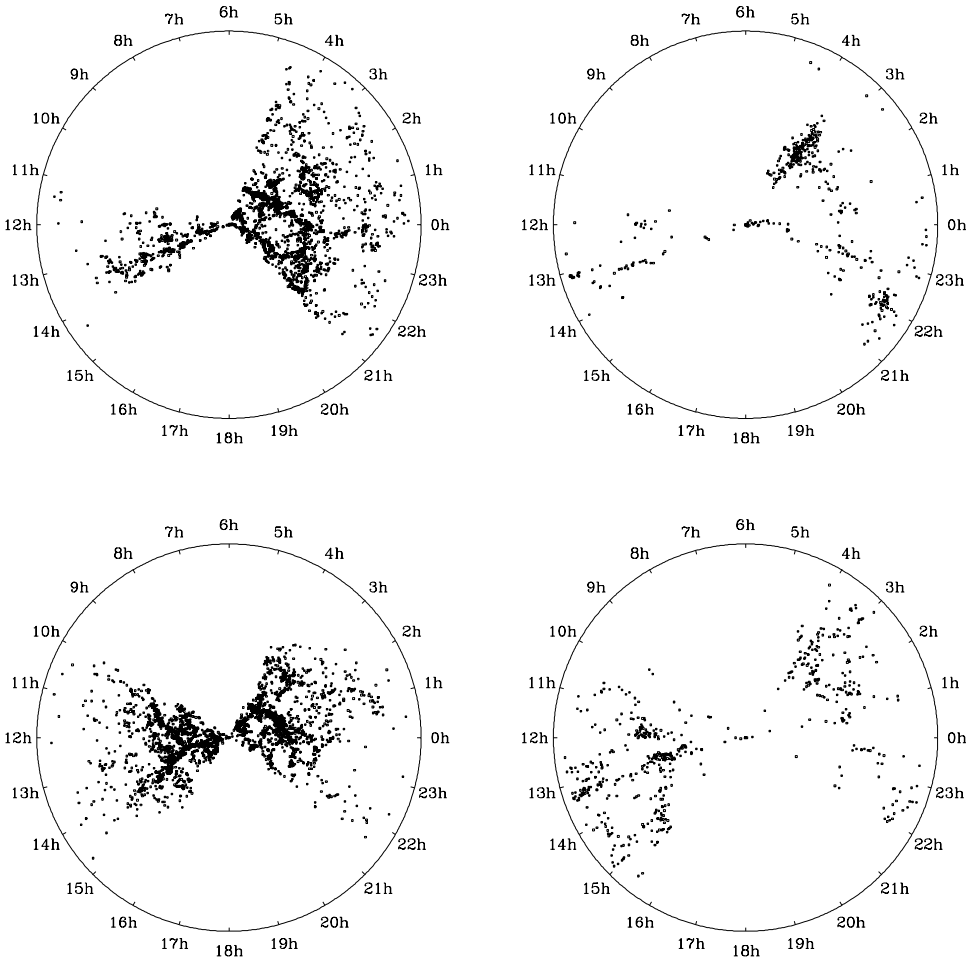
6h
7h
5h
8h
4h
9h
3h
10h
2h
11h
1h
12h
0h
13h
23h
14h
22h
15h
21h
16h
20h
17h
19h
18h

Figure 4

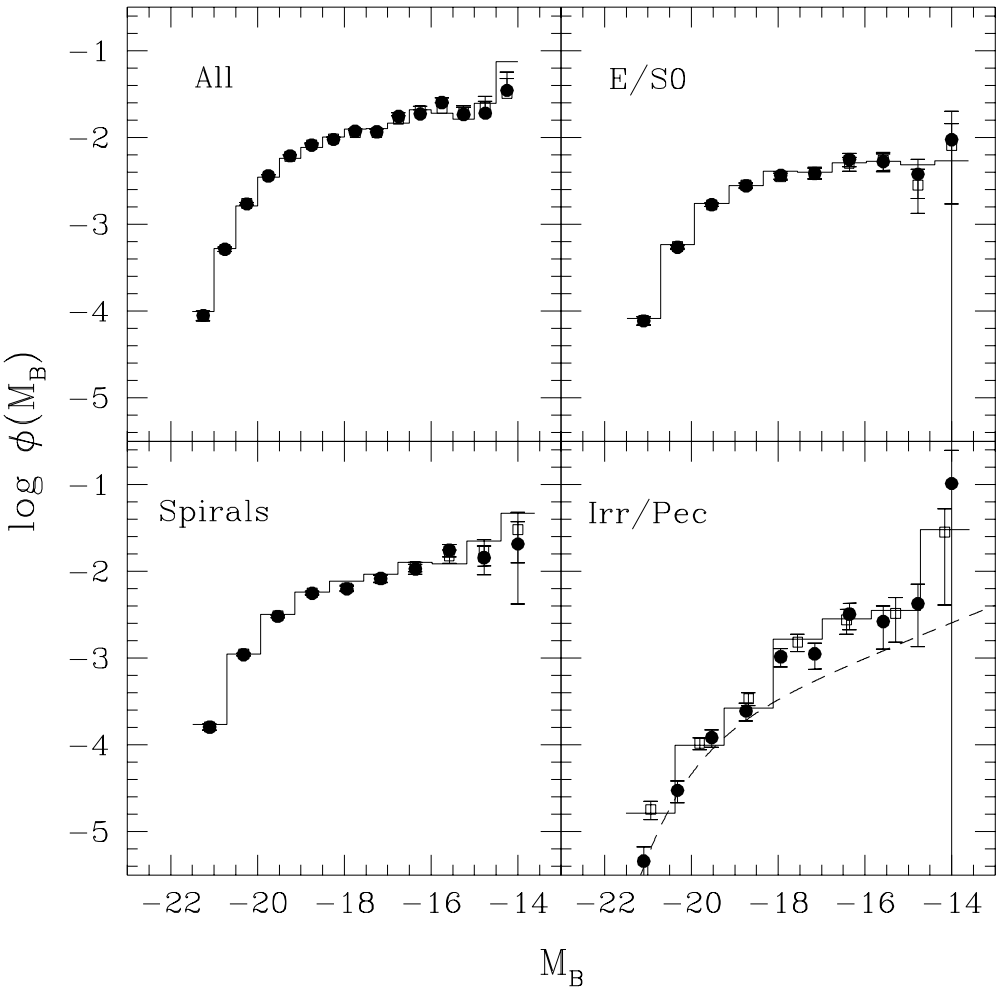

Figure 5

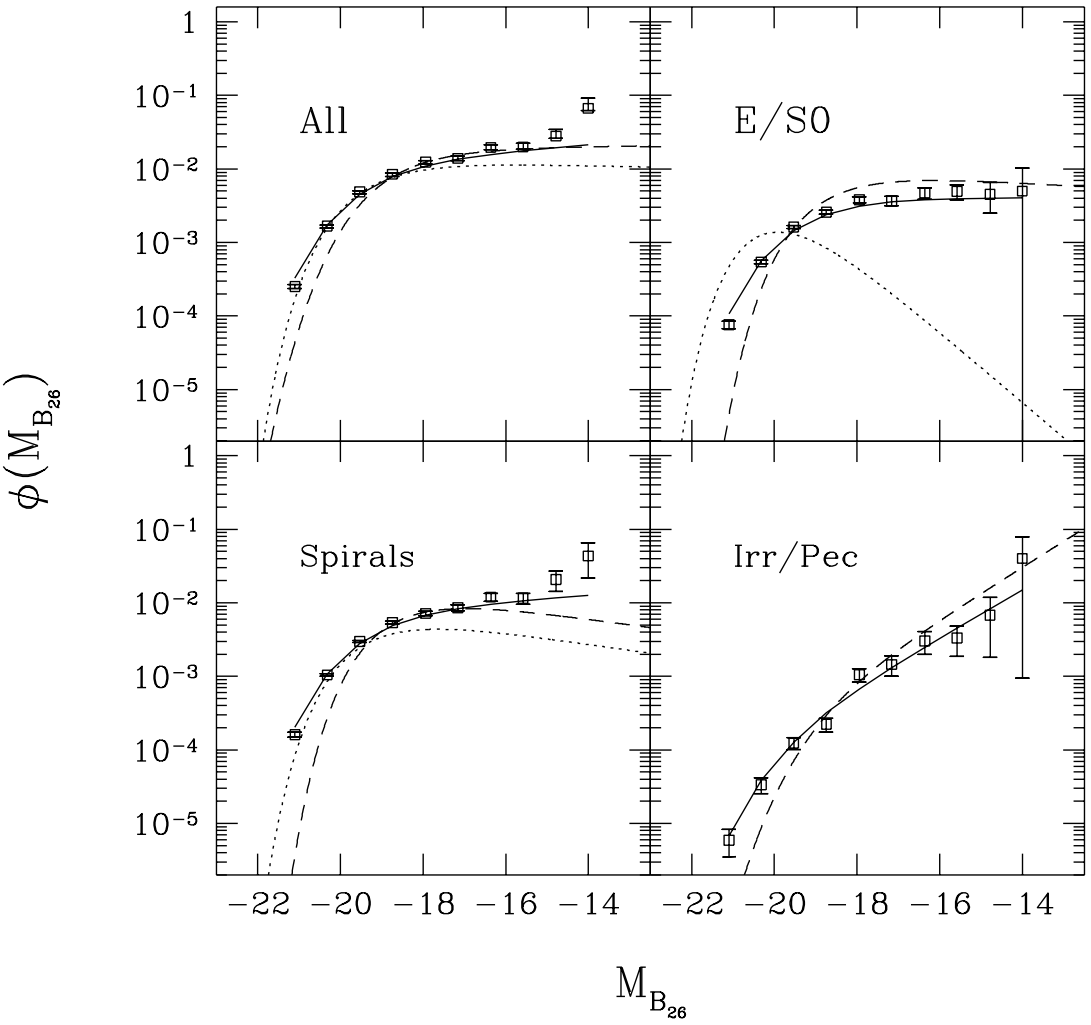
All
E/S0
Spirals
Irr/Pec
1
10^{-1}
10^{-2}
10^{-3}
10^{-4}
10^{-5}
−22 −20 −18 −16 −14
$\phi(M_{B_{26}})$
$M_{B_{26}}$

Figure 6

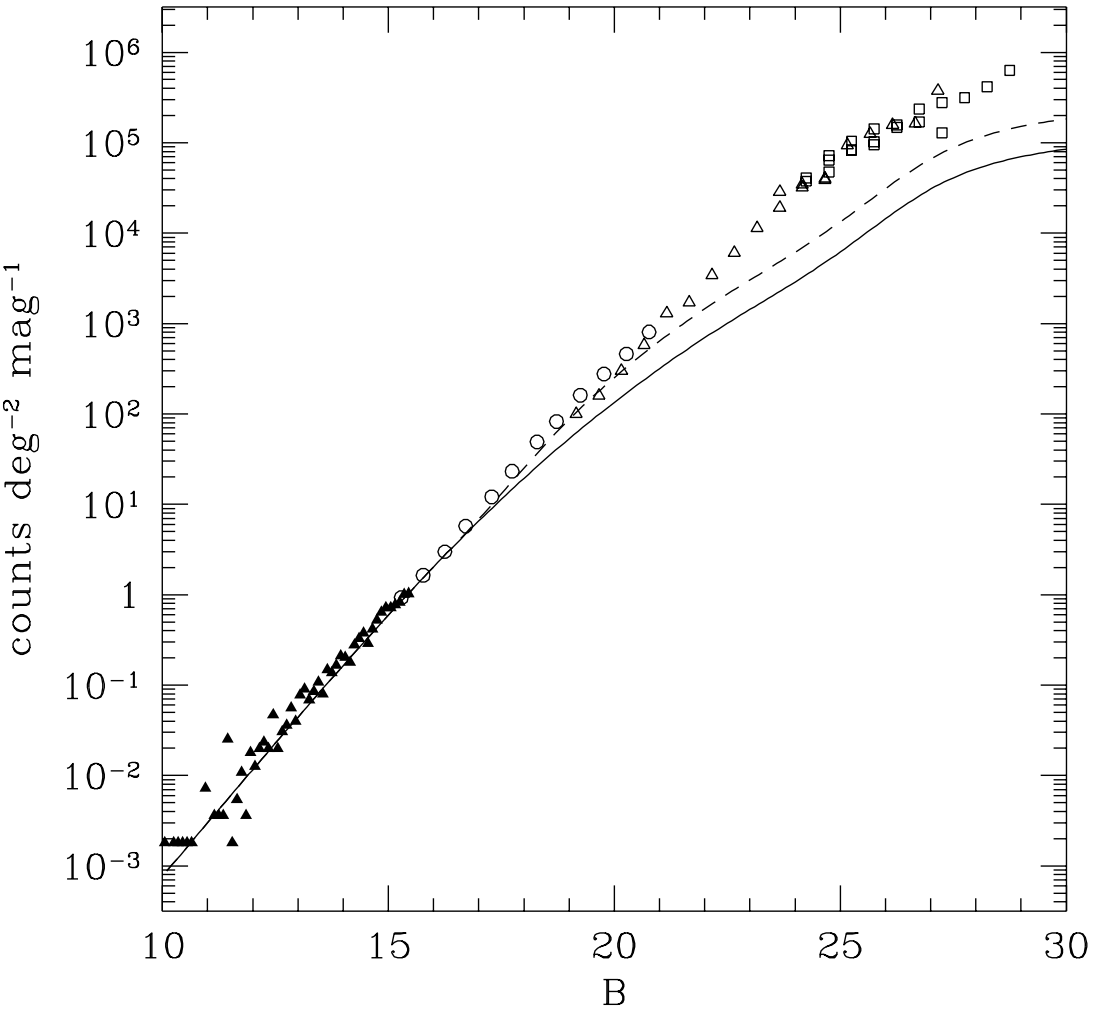
counts deg^{-2} mag^{-1}
10^6
10^5
10^4
10^3
10^2
10^1
1
10^{-1}
10^{-2}
10^{-3}
10
15
20
25
30
B

Figure 7

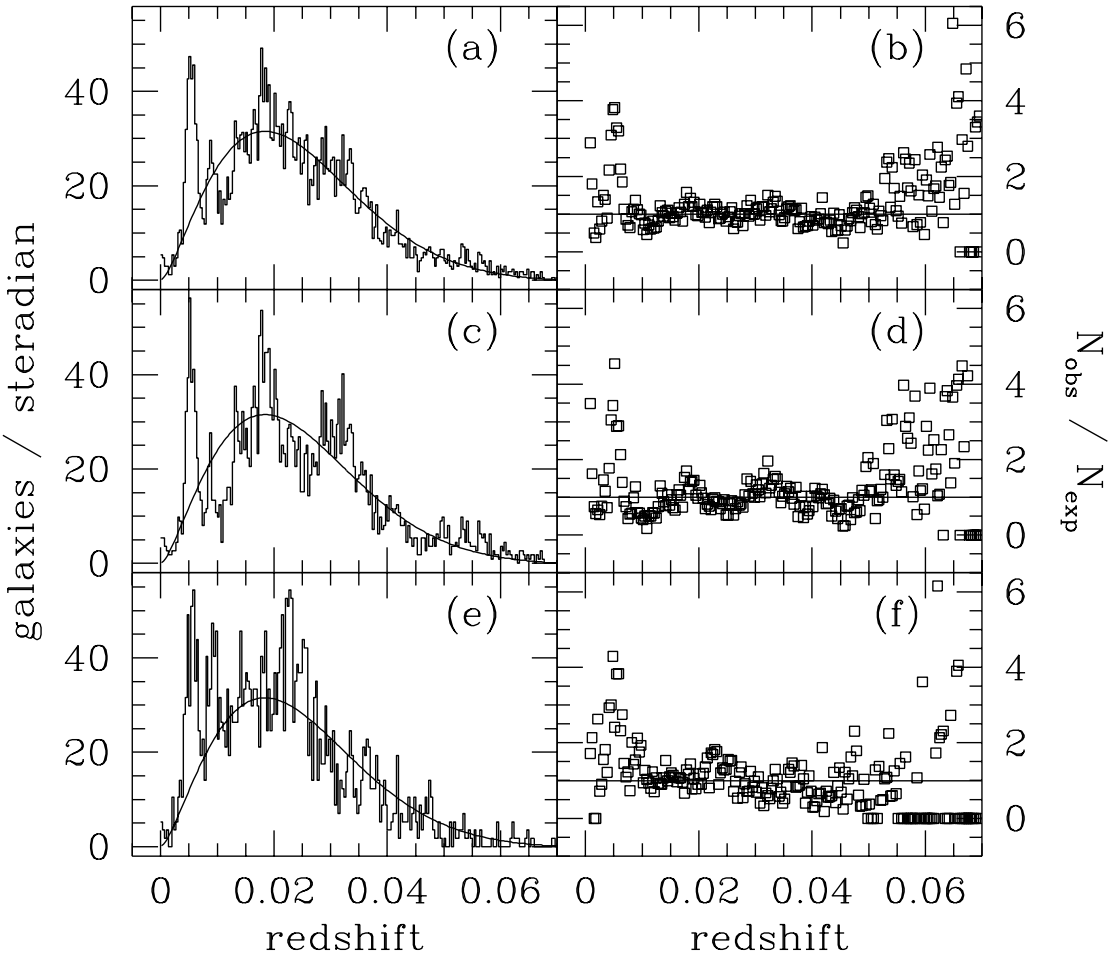
(a)
(b)
(c)
(d)
(e)
(f)
galaxies / steradian
N_{obs} / N_{exp}
redshift
redshift
0
20
40
2
4
6
0.02
0.04
0.06

Figure 8

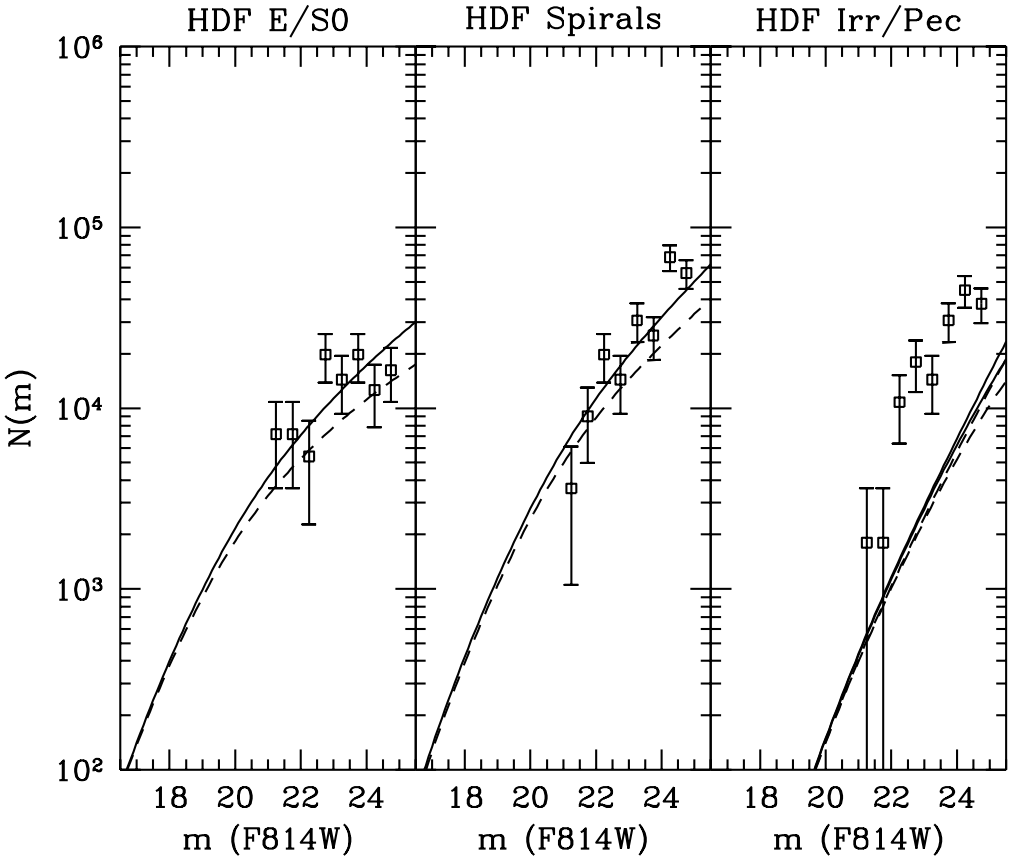
HDF E/S0
HDF Spirals
HDF Irr/Pec
N(m)
10⁶
10⁵
10⁴
10³
10²
18 20 22 24
m (F814W)

Figure 9